# The membrane-linked adaptor FRS2β fashions a cytokine-rich inflammatory microenvironment that promotes breast cancer carcinogenesis

Yasuto Takeuchi[a,1], Natsuko Kimura[b,1], Takahiko Murayama[a,b,1], Yukino Machida[b,c], Daisuke Iejima[b], Tatsunori Nishimura[a,b], Minoru Terashima[d], Yuming Wang[a], Mengjiao Li[a], Reiko Sakamoto[e], Mizuki Yamamoto[f], Naoki Itano[g], Yusuke Inoue[h], Masataka Ito[i], Nobuaki Yoshida[e], Jun-ichiro Inoue[f], Koichi Akashi[j], Hideyuki Saya[k], Koji Fujita[l], Masahiko Kuroda[l], Issay Kitabayashi[c], Dominic Voon[m], Takeshi Suzuki[d], Arinobu Tojo[b], and Noriko Gotoh[a,b,2]

[a]Division of Cancer Cell Biology, Cancer Research Institute, Institute for Frontier Science Initiative, Kanazawa University, Kanazawa 920-1192, Japan; [b]Division of Molecular Therapy, Institute of Medical Science, University of Tokyo, Tokyo 108-8639, Japan; [c]Division of Hematological Malignancy, National Cancer Center Research Institute, Tokyo 104-0045, Japan; [d]Division of Functional Genomics, Cancer Research Institute, Institute for Frontier Science Initiative, Kanazawa University, Kanazawa 920-1192, Japan; [e]Laboratory of Developmental Genetics, Institute of Medical Science, University of Tokyo, Tokyo 108-8639, Japan; [f]Division of Cellular and Molecular Biology, Institute of Medical Science, University of Tokyo, Tokyo 108-8639, Japan; [g]Department of Molecular Biosciences, Faculty of Life Sciences, Kyoto Sangyo University, Kyoto 603-8555, Japan; [h]Department of Diagnostic Radiology, Kitasato University of School of Medicine, Sagamihara City 252-0373, Japan; [i]Department of Anatomy, National Defense Medical College, Tokorozawa 359-8513, Japan; [j]Department of Medicine and Biosystemic Science, Graduate School of Medicine, Kyushu University, Fukuoka 812-8582, Japan; [k]Division of Gene Regulation, Institute of Advanced Medical Research, Keio University, Tokyo 160-8582, Japan; [l]Department of Molecular Pathology, Tokyo Medical University, Tokyo 160-8402, Japan; and [m]Cancer Research Institute, Institute for Frontier Science Initiative, Kanazawa University, Kanazawa 920-1192, Japan

Edited by Tak W. Mak, University of Toronto, Toronto, ON, Canada, and approved August 19, 2021 (received for review February 23, 2021)

**Although it is held that proinflammatory changes precede the onset of breast cancer, the underlying mechanisms remain obscure. Here, we demonstrate that FRS2β, an adaptor protein expressed in a small subset of epithelial cells, triggers the proinflammatory changes that induce stroma in premalignant mammary tissues and is responsible for the disease onset. FRS2β deficiency in mouse mammary tumor virus (MMTV)–ErbB2 mice markedly attenuated tumorigenesis. Importantly, tumor cells derived from MMTV-ErbB2 mice failed to generate tumors when grafted in the FRS2β-deficient premalignant tissues. We found that colocalization of FRS2β and the NEMO subunit of the IκB kinase complex in early endosomes led to activation of nuclear factor–κB (NF-κB), a master regulator of inflammation. Moreover, inhibition of the activities of the NF-κB–induced cytokines, CXC chemokine ligand 12 and insulin-like growth factor 1, abrogated tumorigenesis. Human breast cancer tissues that express higher levels of FRS2β contain more stroma. The elucidation of the FRS2β–NF-κB axis uncovers a molecular link between the proinflammatory changes and the disease onset.**

premalignant inflammation | breast cancer | NF-κB | cancer-associated fibroblasts | FRS3

Breast cancer is the most common cause of cancer among women (1). It is therefore imperative to prevent the onset of breast cancer; however, preventive strategies that are free from significant side effects remain to be established (2).

It has been long held that inflammatory changes contribute to the onset of the disease (3). Epidemiological evidence such as the protective effects of antiinflammatory drugs, including aspirin, provides additional support to this notion (2). In addition, recent studies have revealed that obesity causes inflammatory changes in adipose tissues, and this in turn increases the risk of breast cancer (4). Given that many nonobese women also suffer from breast cancer, the precise molecular mechanisms through which inflammatory changes promote mammary carcinogenesis awaits a thorough investigation. The delineation of the mechanisms is therefore a pressing medical need, as it may hold the key to the development of effective preventive strategies.

Mammary tissues consist of multiple branching tubules that terminate with lobuli (5). The epithelium comprises two major cell layers: luminal cells that have a cuboidal shape and surround the inner lumen and highly elongated myoepithelia on the other side. During pregnancy, luminal cells rapidly expand and form alveoli for milk secretion. Based on the pathological analysis, it is believed that human breast cancer initiates and gradually progresses for more than 30 y (6, 7). It would be difficult to investigate the molecular mechanisms of inflammatory changes during the onset of breast cancer by using numerous human biopsy samples. It is thus useful to analyze mouse mammary tumor models that recapitulate the process of tumor development.

A subset of breast cancer tissues expresses ErbB2 (also known as HER2), a receptor tyrosine kinase, at a high level

## Significance

**Human breast cancer develops after a long period of latency under premalignant conditions. Strategies to target the premalignant conditions have yet to materialize since the molecular mechanisms remain obscure. Here, we discovered that FRS2β, expressed in a subset of mammary epithelial cells, directly activates nuclear factor–κB (NF-κB) and drives the initiation and promotion of the stroma-rich premalignant conditions. The FRS2β-triggered activation of NF-κB takes place in the early endosomes, the organelles, which have not been believed to be a major place for NF-κB signaling. The endosome signaling should be a novel focus for targeting therapy for prevention of breast cancer. This work paves a new way to develop preventive strategies of breast tumor development.**

Author contributions: Y.T., N.K., T.M., Y.M., N.I., Y.I., J.-i.I., K.A., H.S., K.F., M.K., I.K., T.S., A.T., and N.G. designed research; Y.T., N.K., T.M., Y.M., D.I., T.N., M.T., Y.W., M.L., R.S., M.I., K.F., M.K., T.S., and N.G. performed research; R.S. and N.Y. contributed new reagents/analytic tools; Y.T., N.K., T.M., Y.M., D.I., T.N., M.T., M.I., K.F., M.K., T.S., and N.G. analyzed data; and Y.T., N.K., T.M., D.V., and N.G. wrote the paper.

The authors declare no competing interest.

This article is a PNAS Direct Submission.



[1]Y.T., N.K., and T.M. contributed equally to this work.

[2]To whom correspondence may be addressed. Email: ngotoh@staff.kanazawa-u.ac.jp.

This article contains supporting information online at http://www.pnas.org/lookup/suppl/doi:10.1073/pnas.2103658118/-/DCSupplemental.

Published October 18, 2021.

(8, 9). The mouse mammary tumor virus (MMTV)–ErbB2 transgenic mice model the stepwise initiation and development of human breast cancer through the overexpression of ErbB2 in mammary tissues (10, 11). This follows clinicopathological data that show ErbB2 overexpression in a subset of lesions of human breast cancer from the initiation stage (12). Activated ErbB2s are transported into the early endosomes, serving as platforms for receptor signaling, from the plasma membrane (13, 14). In our earlier studies, we reported that an adaptor protein FRS2β (also known as FRS3) is localized in the membrane via its N-terminal myristylation signal and constitutively binds to the ErbB2 receptor (15). FRS2β appears to negatively regulate ErbB2 extracellular signal–regulated kinase (ERK) signaling. Although FRS2β is abundantly expressed in the brain (16, 17), we observed that its expression in other tissues is highly restricted to a few epithelial cells (16).

The nuclear factor–κB (NF-κB) family of transcription factors are chief orchestrators of cellular and tissue inflammation. Not surprisingly, it has been implicated in many aspects of cancer biology (3). A variety of proinflammatory cytokines including CXC chemokine ligand (CXCL) 12 are able to activate NF-κB. In addition, ErbB2 appears to activate NF-κB in patient-derived breast cancer cells (18). Stimulation of the cytokine receptors leads to activation of the IκB kinase (IKK) complex, which is composed of two catalytic subunits, IKK-α and IKK-β, and a scaffolding subunit, NEMO (also known as IKK-γ). The IKK complex phosphorylates NF-κB–bound IκBs, thereby targeting them for proteasomal degradation and liberating NF-κB dimers that are composed of RelA (also known as p65) and p50 to enter the nucleus and mediate transcription of target genes.

In this study, we found that FRS2β is expressed in a small subset of luminal cells that includes progenitor cells in mammary tissues. Although FRS2β-deficient mice showed no gross abnormality and only modest reduction of pregnancy-induced expansion of alveolar cells, mammary tumorigenesis was greatly decreased in a background of MMTV-ErbB2 mice. We found that FRS2β and NEMO were frequently colocalized on the early endosomes in macroscopically normal luminal cells. We posit that this interaction is a pivotal node in the NF-κB activation by ErbB2 at the initiation of mammary carcinogenesis. Through this pathway, numerous cytokines are induced, leading to the chronic inflammatory changes. In particularly, we showed NF-κB–induced insulin-like growth factor (IGF) 1 and CXCL12 play important roles for maintenance of cancer stem-like cells (CSCs) that contribute to tumor initiation in vivo and for mobilization of cancer-associated fibroblasts (CAFs), the most frequent component of stroma (19), respectively. In the FRS2β-deficient mammary tissues, such inflammatory changes are hardly observed. Our findings have uncovered a critical molecular link between tissue inflammation and the neoplastic changes that prelude the onset of breast cancer. Given that FRS2β appears to have only a limited role in physiological conditions, the FRS2β pathway may be targetable without significant side effects to prevent tumorigenesis before the onset of the disease.

## Results

**FRS2β Is Expressed in a Small Subset of Luminal Cells and Is Required for Tumor Stroma Formation.** To examine the role of FRS2β in vivo, we mutated *Frs2β* in mice by gene targeting (*SI Appendix*, Fig. S1 *A* and *B*). FRS2β is known to be expressed abundantly in brain tissues (16, 17). Immunoblotting of brain lysate confirmed that the mutant mice were deficient for FRS2β protein by using the anti-FRS2β antibody, which we previously evaluated the specificity for immunoblotting, immunofluorescence, and immunohistochemistry (20) (*SI Appendix*, Fig. S1*C*). The genotype frequencies of offspring born to the heterozygous breeding pairs were in agreement with Mendelian ratio (*SI Appendix*, Fig. S1*D*). The mutant mice grew normally and were fertile, with no gross abnormalities. *Frs2β* promoter activity was detected by β-galactosidase (LacZ) staining of the heterozygous for the *Frs2β* mutant allele (*SI Appendix*, Fig. S1*A*). In the adult brain, the staining was observed in neural cells in cerebral cortex and hippocampus and purkinje cells in cerebellum, for example (*SI Appendix*, Fig. S1 *E* and *F*). Similarly, immunohistochemistry with anti-FRS2β showed cytoplasmic staining in neural cells in hippocampus, as reported previously (20) (*SI Appendix*, Fig. S1*G*). In the mature female mammary tissues, the abundance of *Frs2β* transcript increased significantly during pregnancy and lactation and then decreased during the involution period after weaning (*SI Appendix*, Fig. S1*H*). LacZ-stained cells were observed in several alveolar cells in mammary tissues during lactation period (Fig. 1 *A* and *B*). Immunohistochemistry revealed that FRS2β was expressed in a small subset of luminal cells that are positive for cytokeratin 18, a luminal cell marker (21) (Fig. 1 *C*–*E*). However, FRS2β was not expressed in myoepithelial cells that are positive for cytokeratin 14, a myoepithelial cell marker (Fig. 1 *C* and *E* and *SI Appendix*, Fig. S1*I*). These data suggest that a subset of luminal cells in the mammary gland express FRS2β.

Whole-mount staining of the mammary gland revealed no gross structural abnormality in the mutant mice (*SI Appendix*, Fig. S2*A*). There were no significant differences in number and length of the mammary tree branches (*SI Appendix*, Fig. S2 *B* and *C*). Although we observed modest reduction of alveolar cells in *Frs2β* $(^{-/-})$ mammary tissues during lactation period (*SI Appendix*, Fig. S2 *D* and *E*), the production of milk of *Frs2β* $(^{-/-})$ mammary tissues should be sufficient for raising pups, since there were no differences in body weight of offspring born to either *Frs2β* $(^{+/+})$ or *Frs2β* $(^{-/-})$ mother mice (*SI Appendix*, Fig. S2*F*).

Although *Frs2β* $(^{-/-})$ mice have very minor phenotype in normal conditions, we hypothesized that FRS2β is involved in pathological conditions, such as tumorigenesis. To test this hypothesis, we used MMTV-ErbB2 (+) mammary tumor model mice. We found that the number of FRS2β–positive luminal cells in the mammary gland during lactation period was greater in MMTV-ErbB2 (+) mice than in MMTV-ErbB2 (−) mice (*SI Appendix*, Fig. S2 *G* and *H*). We crossed *Frs2β* mutant mice with the MMTV-ErbB2 (+) mice to generate MMTV-ErbB2 (+)/*Frs2β* $(^{+/+})$, MMTV-ErbB2 (+)/*Frs2β* $(^{\pm})$, and MMTV-ErbB2 (+)/*Frs2β* $(^{-/-})$ mice hereafter referred to as *Frs2β* $(^{+/+})$, *Frs2β* $(^{\pm})$, and *Frsβ* $(^{-/-})$, respectively. We detected palpable tumors in *Frs2β* $(^{+/+})$ mice at 23.4 ± 1.9 wk after birth, and 83% of mice had tumors ($n = 8$) after experiencing pregnancy and subsequent lactation after the age of 8 wk. On the other hand, tumors became palpable in virgin *Frs2β* $(^{+/+})$ mice at 32.6 ± 2.6 wk, and only 23.4% of mice had tumors ($n = 8$) (i.e., later and at a lower probability). Since pregnancy and subsequent lactation seem to be required for efficient tumorigenesis, we analyzed mice after pregnancy and lactation (Fig. 1*F*). We used MRI, which is sufficiently sensitive to detect very small cell masses, even those with 1-mm diameters (22). We began to observe small tumors (>5 mm in diameter) 5 to 8 wk after commencement of measurement (19 to 22-wk-old mice) (*SI Appendix*, Fig. S3*A*). Strikingly, the tumor growth rate was much lower in *Frs2β* $(^{-/-})$ mice than in *Frs2β* $(^{+/+})$ mice (Fig. 1 *G* and *H*), although tumor incidence was similar: 83.2% ($n = 18$) in *Frs2β* $(^{+/+})$ and 88.2% ($n = 17$) in *Frs2β* $(^{-/-})$. This observation indicates that FRS2β plays important roles in mammary tumorigenesis.

Histological examination revealed that *Frs2β* $(^{+/+})$ tumors contained ample stroma, reminiscent of human breast cancer tissues (23) (Fig. 1 *I*, *Upper*, and *SI Appendix*, Fig. S3*B*). By

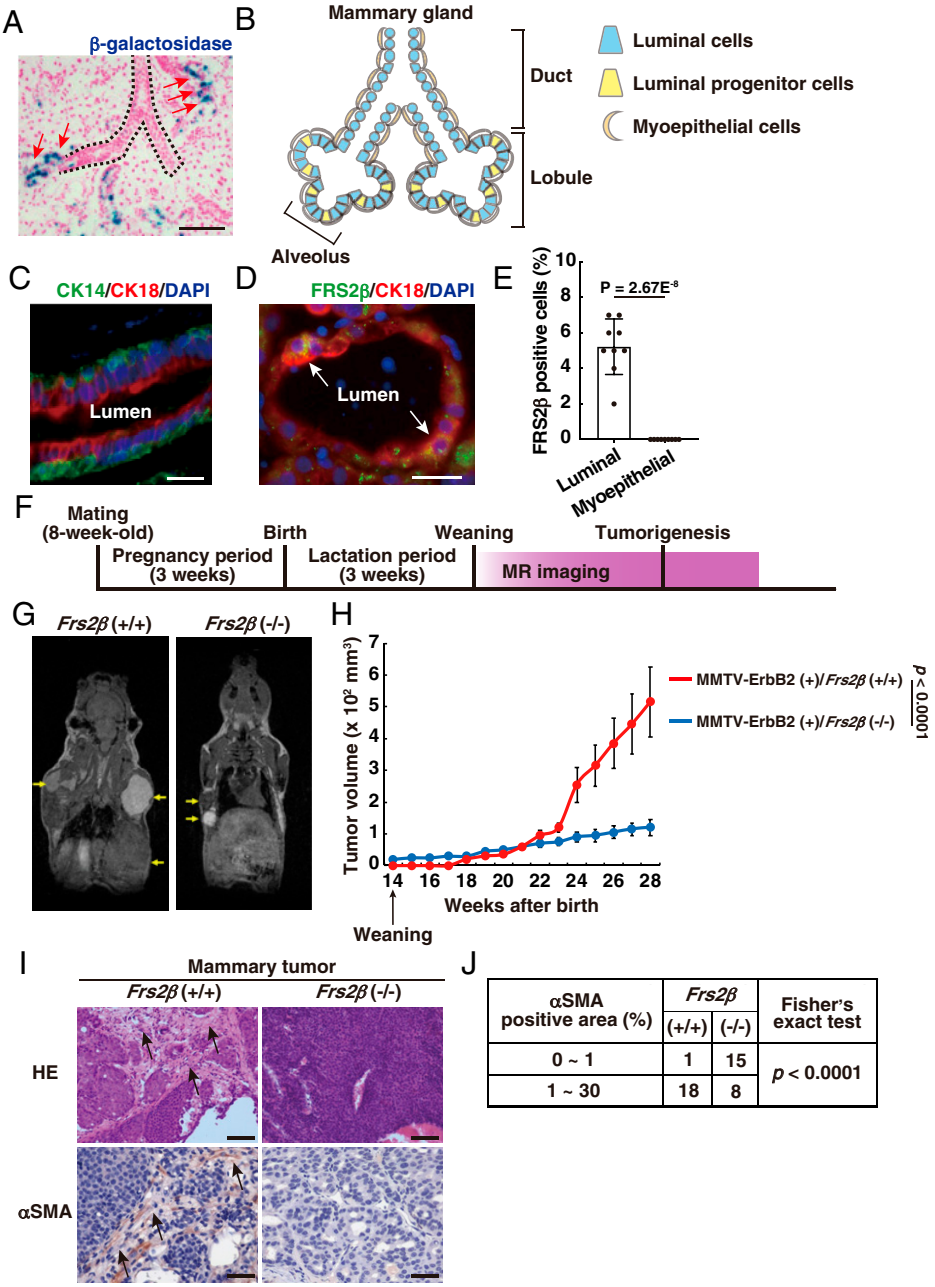


J

| αSMA positive area (%) | Frs2β (+/+) | Frs2β (-/-) | Fisher's exact test |
|---|---|---|---|
| 0 ~ 1 | 1 | 15 | $p < 0.0001$ |
| 1 ~ 30 | 18 | 8 | |

**Fig. 1.** FRS2β is expressed in a subset of luminal epithelial cells in mammary tissues, and deficiency of FRS2β greatly delays mammary tumorigenesis. (*A*) Representative images of β-galactosidase staining of mature female mammary glands from mice heterozygous for the *Frs2β* mutant allele at 16.5 d of pregnancy. Red arrows indicate FRS2β-positive cells. (*B*) Schematic of the mammary glands. Many branching ducts are surrounded by an inner layer of luminal epithelial cells including luminal progenitor cells and an outer layer of myoepithelial cells. (*C*) Representative images of immunofluorescence staining of female mammary glands using antibodies against cytokeratin (CK) 18 and CK14. Nuclei were stained by DAPI. (Scale bar, 25 μm.) (*D*) Representative images of immunofluorescence staining of female mammary glands at 16.5 d of pregnancy using antibodies against FRS2β and CK18. Nuclei were stained by DAPI. Arrows indicate FRS2β-expressing cells. (Scale bar, 25 μm.) (*E*) Quantification of the percentage of FRS2β–positive cells to total number of epithelial cells. $n = 9$ random fields for each cell type. $n = 3$ mice. Statistical significance was determined by unpaired, two-tailed Student's *t* test. Results are shown as means ± SD. (*F*) Schematic of analysis of tumorigenesis. MR, magnetic resonance. (*G*) Representative MRI of mammary tumors, shown in the frontal planes of the 28-wk-old mice. Top is head and Bottom is abdomen. Yellow arrows indicate tumors. (*H*) Tumor growth in MMTV-ErbB2 (+)/*Frs2β* ($^{+/+}$) and MMTV-ErbB2 (+)/*Frs2β* ($^{-/-}$) mice. Tumor sizes were measured once a week for 14 wk. $n = 15$ mice per genotype. Statistical significance was determined by two-way ANOVA with Bonferroni correction. Results are shown as means ± SD. (*I*) Representative images of hematoxylin/eosin (HE) staining of mammary tumors derived from 22-wk-old mice (*Top*). Arrows indicate tumor stroma. (Scale bar, 100 μm.) Representative images of immunohistochemical staining of mammary tumors derived from 22-wk-old mice using antibodies against αSMA (*Bottom*). (Scale bar, 50 μm.) (*J*) Quantification of the percentage of αSMA-positive stroma area within total (stroma and tumor) area derived from tumors of 22 to ~28-wk-old mice. $n = 19$ for *Frs2β* ($^{+/+}$) tumor specimen and $n = 23$ for *Frs2β* ($^{-/-}$) tumor specimen. All the β-galactosidase–staining data and immunohistochemical analysis shown in this figure are representative of at least three biologically independent animals/experiments.

contrast, very little stroma was observed in *Frs2β* ($^{-/-}$) tumors. High levels of smooth muscle actin (SMA)–positive CAFs were present in the stroma of *Frs2β* ($^{+/+}$) tumors but not in *Frs2β* ($^{-/-}$) tumors (Fig. 1 *I*, *Lower* and *J*). The tumor stroma is a major component of the tumor microenvironment. We next analyzed the amount of blood vessels, another important component of the tumor microenvironment, by measuring the amount of CD31-positive endothelial cells. We found that the amount of CD31-positive endothelial cells was significantly smaller in *Frs2β* ($^{-/-}$) tumors than in *Frs2β* ($^{+/+}$) tumors (*SI Appendix*, Fig. S3 *C* and *D*). These results indicate that FRS2β is required for formation of tumor stroma that includes blood vessels.

**FRS2β Plays Important Roles in Creating the Premalignant Mammary Tissue Microenvironment Required for Tumorigenesis.** We next investigated if FRS2β plays roles in creating the mammary tissue microenvironment required for tumorigenesis prior to tumor formation. To test this hypothesis, we performed xenograft experiments in which *Frs2β* ($^{+/+}$) tumor cells were inoculated into 8-wk-old young virgin premalignant mammary tissues of *Frs2β* ($^{+/+}$) and *Frs2β* ($^{-/-}$) mice. We first removed the *Frs2β* ($^{+/+}$) tumors (~1 cm in diameter) from MMTV-ErbB2 mice and cultured the tumor cells as spheres in serum-free suspension in sphere culture medium with a cytokine mixture, as CSCs are enriched under these conditions (24, 25) (Fig. 2*A*). To facilitate tumorigenesis, we used these tumor sphere cells for xenografts. After we made single-cell suspension from the tumor spheres, we inoculated them into 8-wk-old *Frs2β* ($^{+/+}$) and *Frs2β* ($^{-/-}$) virgin mammary tissues and monitored tumorigenesis (Fig. 2*A*). Strikingly, while large tumors formed rapidly in transplanted *Frs2β* ($^{+/+}$) mice, only very small cell masses (<3 mm in diameter) were observed in *Frs2β* ($^{-/-}$) mammary tissues (Fig. 2 *B* and *C* and *SI Appendix*, Fig. S4 *A* and *B*). Limiting dilution assay revealed that no tumor-initiating ability was observed in tumor cells inoculated in *Frs2β* ($^{-/-}$) mammary tissues (Fig. 2 *D* and *E*). These results indicate that tumor cells grew well in the *Frs2β* ($^{+/+}$) mammary tissue microenvironment but not in the *Frs2β* ($^{-/-}$) mammary tissue microenvironment. On the other hand, tumors did not form when *Frs2β* ($^{+/+}$) tumor cells were inoculated into the *Frs2β* ($^{+/+}$) male mammary fat pads (*SI Appendix*, Fig. S4*C*). We also inoculated 10,000 *Frs2β* ($^{+/+}$) tumor cells subcutaneously into the flanks of *Frs2β* ($^{+/+}$) female mice and found no palpable tumors after 35 d. From these findings, we confirmed that the *Frs2β* ($^{+/+}$) female mammary tissue microenvironment is essential for tumorigenesis. Therefore, premalignant mammary gland cells expressing FRS2β create a microenvironment that is essential for tumorigenesis.

**Ample Amounts of Cytokines, Including IGF1 and CXCL12, Are Expressed in the Premalignant Mammary Epithelial Cells in an FRS2β-Dependent Manner, and FRS2β Is Expressed in a Part of Luminal Progenitor Cells.** Next, we examined the molecular mechanisms by which FRS2β expressed in luminal cells create a microenvironment that is essential for tumorigenesis. For this purpose, we cultured *Frs2β* ($^{+/+}$) and *Frs2β* ($^{-/-}$) premalignant mammary epithelial cells derived from 8- to 12-wk-old mice and compared their transcriptomic profiles using DNA microarrays. Gene set enrichment analysis revealed that gene sets related to NF-κB targets, stem cell function, and stroma were enriched in *Frs2β* ($^{+/+}$) cells relative to *Frs2β* ($^{-/-}$) cells (Fig. 2*F*). In contrast, the ERK pathway–related gene set was up-regulated in *Frs2β* ($^{-/-}$) cells relative to *Frs2β* ($^{+/+}$) cells, which was confirmed by increased expression levels of phosphorylated ERK1/2 in *Frs2β* ($^{-/-}$) cells by immunoblotting (*SI Appendix*, Fig. S4 *D* and *E*). This was expected because FRS2β inhibits ERK signaling (15).

Many genes encoding cytokines were up-regulated in *Frs2β* ($^{+/+}$) cells (*SI Appendix*, Table S1); among them, the top 10 genes at higher expression levels in *Frs2β* ($^{+/+}$) cells than in *Frs2β* ($^{-/-}$) cells were indicated (Fig. 2*G*). We then focused on *Igf1* and *Cxcl12*, both of which were included in the gene sets related to NF-κB targets. *Igf1* and *Cxcl12* were also included in the gene sets related to stem cell function and stroma, respectively. qPCR confirmed that *Igf1* and *Cxcl12* transcripts were expressed at higher levels in *Frs2β* ($^{\pm}$) than in *Frs2β* ($^{-/-}$) premalignant mammary epithelial cells (Fig. 2*H*). Immunohistochemistry revealed that the protein levels of IGF1 and CXCL12 were higher in the cytoplasm of *Frs2β* ($^{+/+}$) premalignant luminal cells than in *Frs2β* ($^{-/-}$) cells (Fig. 2 *I–L* and *SI Appendix*, Fig. S5 *A* and *B*). Inflamed areas in which immune cells were accumulated were observed in the *Frs2β* ($^{+/+}$) premalignant mammary tissues but not in *Frs2β* ($^{-/-}$) premalignant mammary tissues (Fig. 2 *M* and *N* and *SI Appendix*, Fig. S5*C*). These results indicate that the premalignant mammary epithelial cells produce ample amounts of cytokines, including IGF1 and CXCL12, and that cytokine production was significantly reduced in FRS2β-deficient mammary epithelial cells.

To examine whether the up-regulation of these cytokines was due to overexpression of ErbB2, we compared the expression levels of IGF1 and CXCL12 in premalignant mammary tissues between MMTV-ErbB2(−)/*Frs2β* ($^{+/+}$) mice and MMTV-ErbB2(+)/*Frs2β* ($^{+/+}$) mice using immunohistochemistry and qPCR. We observed that the expression levels were up-regulated in MMTV-ErbB2(+)/*Frs2β* ($^{+/+}$) premalignant mammary tissues as compared to those of MMTV-ErbB2(−)/*Frs2β* ($^{+/+}$) mice (*SI Appendix*, Fig. S6 *A–C*). These findings indicate that overexpression of ErbB2 causes up-regulation of IGF1 and CXCL12 in the premalignant mammary tissues.

We next examined in which type of luminal cells FRS2β is expressed. We sorted the mammary epithelial cells derived from 10-wk-old virgin *Frs2β* ($^{+/+}$) or *Frs2β* ($^{-/-}$) mice by their expression of surface markers. It is known that the progenitor cells are enriched in the CD49f$^{low}$/CD24$^{high}$ cell population (26) (*SI Appendix*, Fig. S4 *F*, *Right*, *P3*, and G, *Left*, *P3*) and that the luminal progenitor cells can be enriched by further fractionation with CD61 for the CD49f$^{low}$/CD24$^{high}$/CD61$^{+}$ population (27) (*SI Appendix*, Fig. S4*G*, *Middle*, *P5*). After permealization of the CD49f$^{low}$/CD24$^{high}$/CD61$^{+}$ cells, we next analyzed them by using anti–FRS2β antibody. We observed significant expression of FRS2β in 23.6% cells among the CD49f$^{low}$/CD24$^{+high}$/CD61$^{+}$ luminal progenitor cell population (*SI Appendix*, Fig. S4*G*, *Upper Right*, *P6*). We confirmed that FRS2β was lost in CD49f$^{low}$/CD24$^{high}$/CD61$^{+}$ luminal progenitor cell population derived from *Frs2β* ($^{-/-}$) mammary epithelial cells (*SI Appendix*, Fig. S4*G*, *Lower Right*, *P6*). These data suggest that a subset of luminal progenitor cells in the mammary gland express FRS2β.

We then cultured premalignant mammary epithelial cells as mammospheres in which stem/progenitor cells are enriched (28). We found that the efficiency of mammosphere formation was greater in *Frs2β* ($^{+/+}$) premalignant mammary epithelial cells than in *Frs2β* ($^{-/-}$) cells in several passages (*SI Appendix*, Fig. S4 *H* and *I*). Our findings suggest that FRS2β contributes to growth ability of macroscopically normal mammary stem/progenitor cells.

**The FRS2β-Dependent Increase in IGF1 and CXCL12 Production in Premalignant Mammary Epithelial Cells Promotes Tumor Sphere Formation and CAF Mobilization.** Tumor sphere formation reflects the properties of CSCs, whose growth is dependent on cytokines in the culture (24). To determine whether IGF1 derived from premalignant mammary epithelial cells plays a role in tumor sphere formation, we cultured *Frs2β* ($^{+/+}$) tumor cells under serum-free suspension condition without the standard

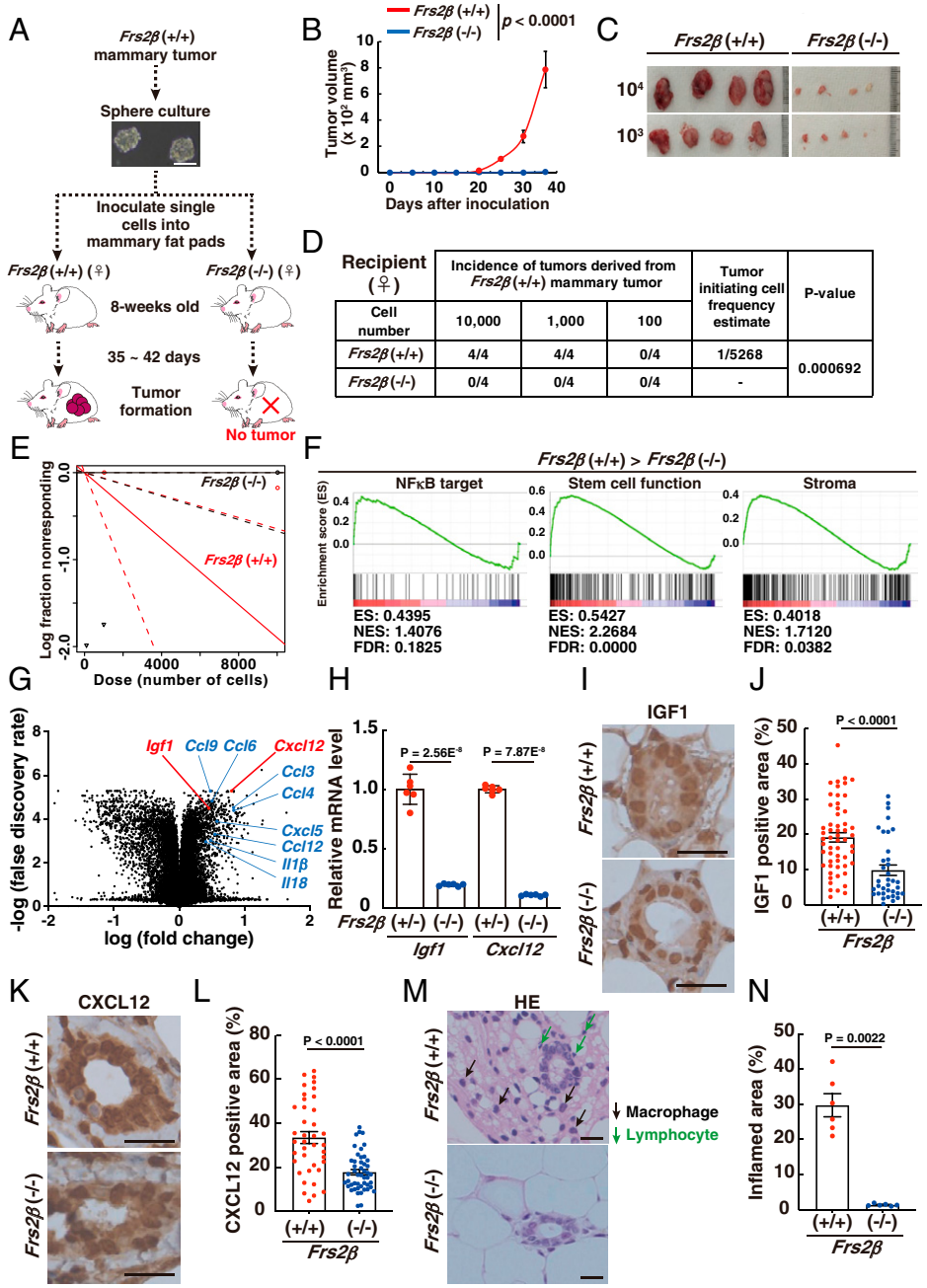


**Fig. 2.** FRS2β-expressing premalignant mammary tissues are essential for tumorigenesis and produce cytokines including IGF1 and CXCL12. (*A*) *Frs2β* ($^{+/+}$) tumor sphere cells cultured for 14 d, as shown by the representative image, and $10^2$, $10^3$, or $10^4$ cells were inoculated into the mammary fat pads of 8-wk-old virgin female *Frs2β* ($^{+/+}$) or *Frs2β* ($^{-/-}$) mice. (Scale bar, 100 μm.) (*B*) Tumor volumes ($10^4$ cells inoculation) were measured. Statistical significance was determined by two-way ANOVA with Bonferroni correction. Results are shown as means ± SD. (*C*) Representative tumors were photographed 35 d after transplantation. $n = 4$ mice for each experiment per genotype. (*D* and *E*) Results of limiting dilution assay of tumors. Tumors larger than 50 $mm^3$ after 35 d were counted. Tumor-initiating cell frequency and *P* values were determined using the Extreme Limiting Dilution Analysis (ELDA) software. (*F*) Gene set enrichment analysis was used to compare gene expression profiles in *Frs2β* ($^{+/+}$) and *Frs2β* ($^{-/-}$) premalignant mammary epithelial cells. Gene sets highly up-regulated in *Frs2β* ($^{+/+}$) cells are shown. ES, enrichment score; FDR, false discovery ratio; and NES, normalized enrichment score. $n = 3$ biologically independent experiments per genotype. (*G*) Volcano plot of gene expression profiles. Fold changes of expression levels in *Frs2β* ($^{+/+}$) premalignant mammary epithelial cells with respect to those of *Frs2β* ($^{-/-}$) cells were calculated. $n = 3$ biologically independent experiments per genotype. (*H*) Expression levels of the indicated gene transcripts were compared between *Frs2β* ($^{\pm}$) and *Frs2β* ($^{-/-}$) mammary epithelial cells using real-time qPCR. Values were normalized to 18S ribosomal RNA, and fold changes were calculated relative to the values of *Frs2β* ($^{\pm}$). Statistical significance was determined by unpaired, two-tailed Student's *t* test. Results are shown as means ± SEM. $n = 6$ biologically independent experiments per genotype. (*I–L*) Representative images of immunohistochemical staining of *Frs2β* ($^{+/+}$) and *Frs2β* ($^{-/-}$) mammary tissues derived from 8-wk-old virgin female mice using antibodies against IGF1 (*I*) and CXCL12 (*K*). (Scale bars, 50 μm.) Quantification of the cytoplasmic stained area within epithelial cells in mammary glands using antibodies against IGF1 (*J*) or CXCL12 (*L*). $n = 56$ cells in *Frs2β* ($^{+/+}$), $n = 36$ cells in *Frs2β* ($^{-/-}$) mammary tissues (*J*), $n = 39$ cells in *Frs2β* ($^{+/+}$), and $n = 49$ cells in *Frs2β* ($^{-/-}$) mammary tissues (*L*). (*M* and *N*) Representative images of hematoxylin/eosin staining of *Frs2β* ($^{+/+}$) and *Frs2β* ($^{-/-}$) mammary tissues derived from 8-wk-old virgin female mice (*M*). (Scale bars, 20 μm.) (*N*) Quantification of the inflamed area within mammary tissues. $n = 6$ random fields per genotype. (*J*, *L*, and *N*) Statistical significance was determined by two-tailed Mann–Whitney *U* test. Results are shown as means ± SEM. All the immunohistochemical analyses in this figure are representative of at least three biologically independent animals.

cytokine mixture in the presence or absence of premalignant *Frs2β* ($^{+/+}$) mammary epithelial cells (Fig. 3*A*). We observed tumor sphere formation by *Frs2β* ($^{+/+}$) tumor cells in the presence of *Frs2β* ($^{+/+}$) premalignant mammary epithelial cells but not in their absence (compare control versus not cocultured in Fig. 3 *B* and *C*). Treatment with an IGF1-neutralizing antibody greatly diminished tumor sphere formation by *Frs2β* ($^{+/+}$) tumor cells cocultured with *Frs2β* ($^{+/+}$) premalignant mammary cells (Fig. 3 *B* and *C*). These findings indicate that IGF1 derived from nearby *Frs2β* ($^{+/+}$) premalignant mammary epithelial cells plays an important role in tumor sphere formation. Thus, IGF1 derived from *Frs2β* ($^{+/+}$) premalignant mammary epithelial cells may support CSC growth.

To determine whether CXCL12 derived from the premalignant mammary epithelial cells plays roles in CAFs, we obtained *Frs2β* ($^{+/+}$) CAFs from the MMTV-ErbB2 mammary tumors. They had spindle morphology and were positively stained by anti-αSMA and anti-vimentin antibodies, which are typical features of CAFs (29) (*SI Appendix*, Fig. S7 *A* and *B*). We cocultured the *Frs2β* ($^{+/+}$) CAFs with *Frs2β* ($^{+/+}$) or *Frs2β* ($^{-/-}$) premalignant mammary epithelial cells (Fig. 3*D*). We observed significantly more migrated CAFs in cocultures with *Frs2β* ($^{+/+}$)

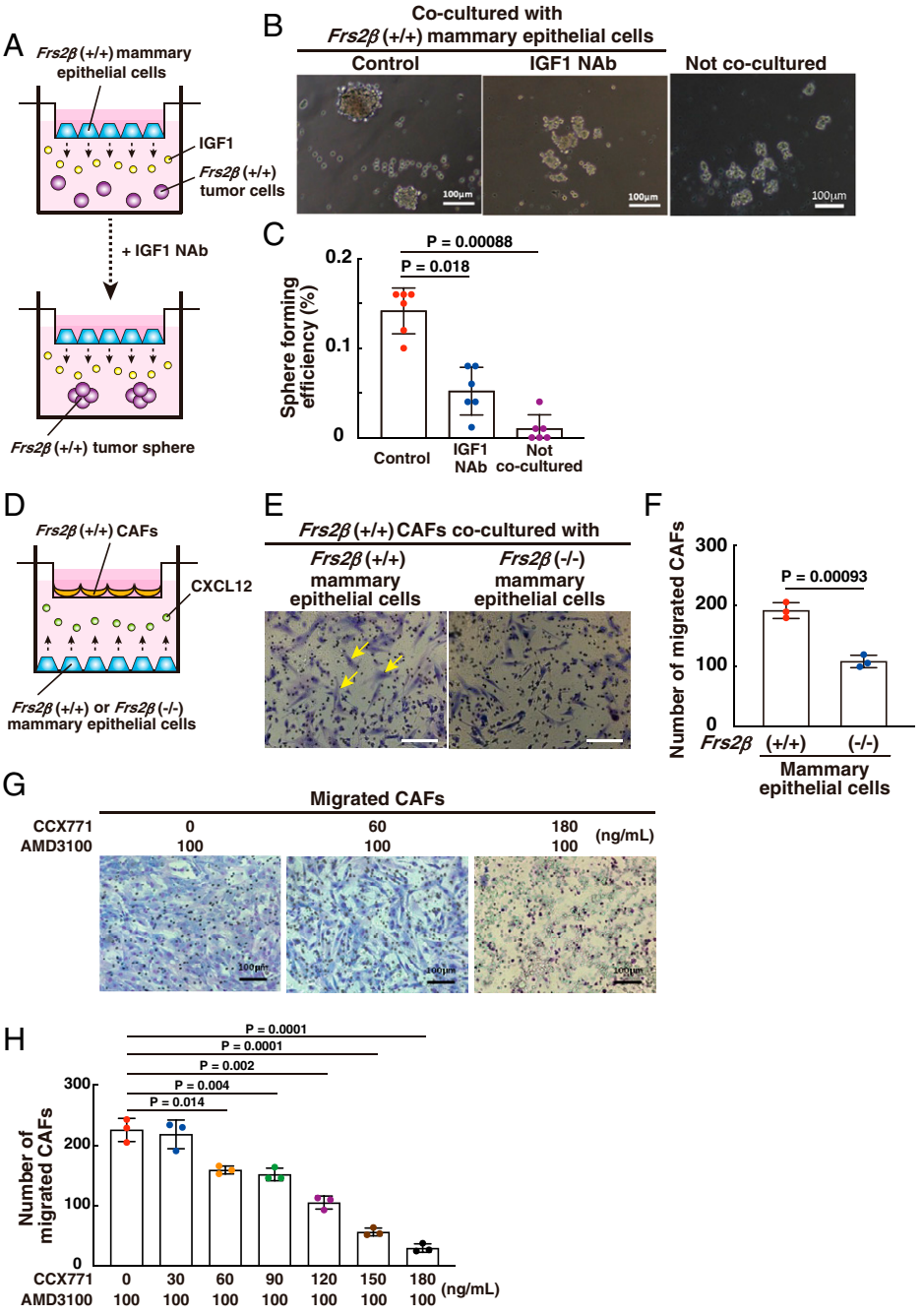


**Fig. 3.** IGF1 and CXCL12 produced by premalignant *Frs2β* ($^{+/+}$) mammary epithelial cells induce tumor spheres and migration of CAFs, respectively. (*A–C*) Schematic of coculture of *Frs2β* ($^{+/+}$) tumor cells to form spheres in the lower chamber with *Frs2β* ($^{+/+}$) premalignant mammary epithelial cells in the upper chamber (*A*). (*B*) Representative images of tumor sphere formation in the presence of *Frs2β* ($^{+/+}$) mammary epithelial cells treated with control IgG (400 nM) (control) or IGF1-neutralizing antibody (NAb) (400 nM) after 7 d of coculture or in the absence of *Frs2β* ($^{+/+}$) mammary epithelial cells after 7 d of culture. (Scale bars, 100 μm.) (*C*) Quantification of tumor sphere–forming efficiency. $n = 3$ mice per group. The results are representative of the four independent experiments. Statistical significance was determined by unpaired, two-tailed Student's *t* test. Results are shown as means ± SD. (*D–F*) Schematic of coculture of *Frs2β* ($^{+/+}$) or *Frs2β* ($^{-/-}$) premalignant mammary epithelial cells in the lower chamber with *Frs2β* ($^{+/+}$) CAFs in the upper chamber (*D*). (*E*) Representative images of migrated *Frs2β* ($^{+/+}$) CAFs cocultured with *Frs2β* ($^{+/+}$) or *Frs2β* ($^{-/-}$) mammary cells after 24 h of coculture. Arrows indicate migrated CAFs. (Scale bar, 20 μm.) (*F*) Quantification of migrated *Frs2β* ($^{+/+}$) or *Frs2β* ($^{-/-}$) CAFs. $n = 3$ mice per genotype. The results are representative of the four independent experiments. Statistical significance was determined by unpaired, two-tailed Student's *t* test. Results are shown as means ± SD. (*G* and *H*) Representative images of migrated *Frs2β* ($^{+/+}$) CAFs cocultured with *Frs2β* ($^{+/+}$) mammary epithelial cells for 24 h. Cells were treated with the indicated concentration of CCX71 and 100 ng/mL AMD3100 (*G*). (Scale bar, 100 μm.) (*H*) Quantification of migrated *Frs2β* ($^{+/+}$) CAFs cocultured with *Frs2β* ($^{+/+}$) mammary epithelial cells for 24 h. Cells were treated with the indicated concentration of CCX71 and 100 μg/mL AMD3100. $n = 3$ mice per group. The results are representative of the four independent experiments. Statistical significance was determined by unpaired, two-tailed Student's *t* test. Results are shown as means ± SD.

premalignant mammary epithelial cells than in those with *Frs2β* ($^{-/-}$) cells (Fig. 3 *E* and *F*). CXCL12 binds to its receptors CXCR4 and CXCR7 (30). Although we did not observe significant effects on the migration of CAFs upon treatment with the CXCR4 inhibitor AMD3100 (100 ng/mL) or the CXCR7 inhibitor CCX771 (100 ng/mL) alone (*SI Appendix*, Fig. S7*C*), a combination of both inhibitors greatly diminished migration of CAFs in a CCX771 dose-dependent manner in the presence of the effective dose of AMD3100 (Fig. 3 *G* and *H* and *SI Appendix*, Fig. S7*D*). Furthermore, we observed increased migration of CAFs by addition of recombinant CXCL12 in the culture media in place of *Frs2β* ($^{+/+}$) premalignant mammary epithelial cells (*SI Appendix*, Fig. S7 *E* and *F*). These findings indicate that CXCL12 derived from nearby *Frs2β* ($^{+/+}$) premalignant mammary epithelial cells contributes to mobilization of CAFs. Taken together, the FRS2β–dependent increases in production of cytokines, including IGF1 and CXCL12, enable premalignant mammary cells to maintain CSC and mobilized CAF at the onset of tumorigenesis.

**FRS2β Triggers Activation of NF-κB to Promote IGF1 and CXCL12 Production in Premalignant Mammary Epithelial Cells.** Next, we examined the molecular mechanisms that induce expression of IGF1 and CXCL2 in premalignant mammary tissues. Since *Igf1* and *Cxcl12* were among list of the identified NF-κB target gene (Fig. 2*F*), we investigated if the activation of NF-κB is involved in the production of these cytokines. To this end, we cultured *Frs-2β* ($^{+/+}$) premalignant mammary epithelial cells and treated them with DHMEQ, a specific inhibitor of NF-κB (Fig. 4*A*). Treatment with DHMEQ inhibited the expression of *Igf1*, *Cxcl12*, and *IκBα*, a well-established NF-κB–inducible gene, in a dose-dependent manner (Fig. 4*B*). We further confirmed

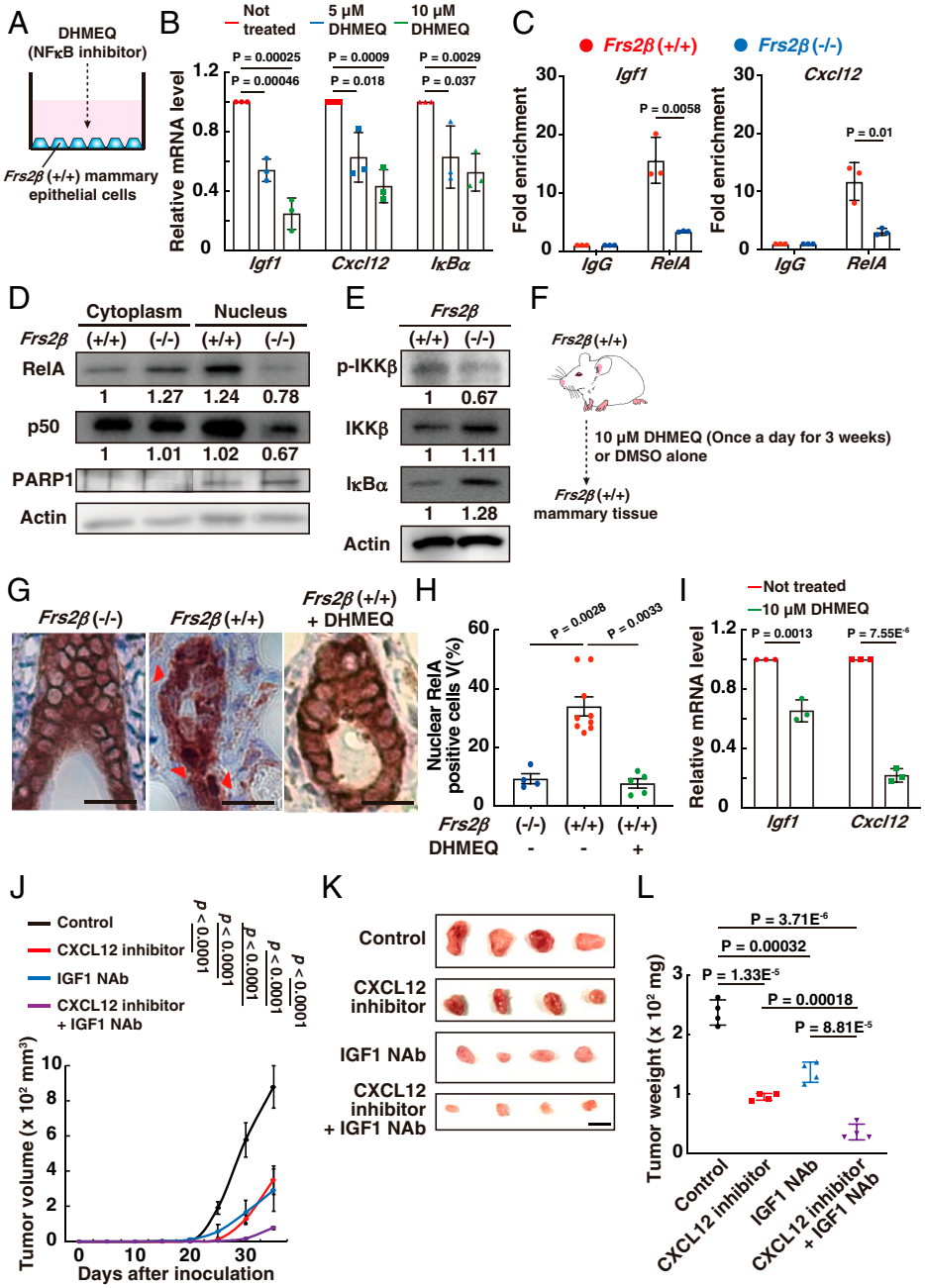


**Fig. 4.** FRS2β-dependent activation of NFκB increases the production of IGF1 and CXCL12 in premalignant mammary tissues and inhibition of IGF1 and CXCL12 abrogates tumorigenesis. (*A* and *B*) Schematic of DHMEQ treatment of cultured *Frs2β* ($^{+/+}$) premalignant mammary epithelial cells in vitro (*A*). (*B*) Expression levels of indicated gene transcripts in *Frs2β* ($^{+/+}$) premalignant mammary epithelial cells treated with the indicated concentration of DHMEQ were compared by qPCR. Values were normalized to 18S ribosomal RNA, and fold changes were calculated relative to the values of control DMSO-treated samples (Not treated). $n = 3$ samples for each condition. (*C*) Chromatin immunoprecipitation assay was performed. Cross-linked cell lysates derived from *Frs2β* ($^{+/+}$) and *Frs2β* ($^{-/-}$) premalignant mammary epithelial cells were immunoprecipitated with the anti-RelA (L8F6) antibody or normal mouse IgG. Enrichment in the immunoprecipitates for the 5' regulatory region of *Igf1* or *Cxcl12* was detected by qPCR, and fold changes were calculated relative to the values of normal mouse IgG. $n = 3$ biologically independent experiments per genotype. (*D*) Immunoblotting analysis of cytoplasmic and nuclear expression levels of the indicated proteins in the lysate of *Frs2β* ($^{+/+}$) or *Frs2β* ($^{-/-}$) mammary tissues. PARP1 was used as a representative protein in nucleus. $n = 3$ per genotype. (*E*) Immunoblotting analysis of the indicated proteins in the lysate of *Frs2β* ($^{+/+}$) or *Frs2β* ($^{-/-}$) mammary tissues. $n = 3$ mice per genotype. (*F*) Schematic of DHMEQ treatment of *Frs2β* ($^{+/+}$) mice in vivo. The mice were intraperitoneally injected with 10 μM/g DHMEQ once a day for 3 wk. $n = 3$ mice for each condition. (*G*) Representative images of immunohistochemical staining with antibodies against RelA for mammary tissues derived from 8-wk-old virgin female mice with or without DHMEQ treatment. Arrowheads indicate nuclear RelA-positive cells. (Scale bar, 50 μm.) (*H*) Quantification of nuclear RelA-positive cells within mammary epithelial cells. $n = 4$ random fields in *Frs2β* ($^{-/-}$), $n = 9$ random fields in *Frs2β* ($^{+/+}$) without treatment with DHMEQ, and $n = 5$ random fields in *Frs2β* ($^{+/+}$) treated with DHMEQ. $n = 3$ samples for each condition. Statistical significance was determined by two-tailed Mann–Whitney *U* test. Results are shown as means ± SEM. (*I*) Expression levels of indicated transcripts in *Frs2β* ($^{+/+}$) mammary tissues with or without DHMEQ treatment. $n = 3$ samples for each condition. (*J–L*) *Frs2β* ($^{+/+}$) tumor sphere cells were inoculated into mammary fat pads of 8-wk-old virgin female *Frs2β* ($^{+/+}$) mice. After 7 d, the mice were intraperitoneally injected with 0.1 μg/g IGF1 antibody once per week and/or 10 μg/g AMD3100 once a day. CCX771 (30 μg/g) was administered orally once a day. CXCL12 inhibitor, combination of AMD3100 and CCX771. $n = 4$ mice for each condition. (*J*) Tumor volumes ($10^4$ cells inoculation) were measured. Statistical significance was determined by two-way ANOVA with Bonferroni correction. (*K*) Representative tumors were photographed on day 42 after transplantation. (Scale bar, 1 cm.) (*L*) Scatter plots of the weights of the removed tumors are shown. (*B, C, I,* and *L*) Statistical significance was determined by unpaired, two-tailed Student's *t* test. Results are shown as means ± SD. (*D* and *E*) Actin was used as a loading control. Intensities of the bands were calculated by using ImageJ software. All the immunoblotting data and immunohistochemical analysis shown in this figure are representative of at least three biologically independent animals.

these results by using two unrelated NF-κB inhibitors, TPCA-1 and SC514. Treatment with TPCA-1 or SC514 inhibited the expression of *Igf1*, *Cxcl12*, and *IκBα* in a dose-dependent manner, similar to treatment with DHMEQ (*SI Appendix*, Fig. S8). We next searched potential NF-κB binding sites in the 5′ regulatory regions of *Igf1* and *Cxcl12* genes by using ChIP-Atlas (http://chip-atlas.org) and found them in each region. Chromatin immunoprecipitation assay showed that RelA, an NF-κB subunit, was strongly recruited to the 5′ regulatory regions of *Igf1* and *Cxcl12* genes in *Frs-2β* ($^{+/+}$) premalignant mammary epithelial cells compared to those of *Frs-2β* ($^{-/-}$) (Fig. 4*C*). This suggests that NF-κB activation plays important roles in the expression of IGF1 and CXCL12 in premalignant mammary epithelial cells.

We then examined activation of NF-κB in premalignant mammary tissues in vivo. Immunoblotting of lysates from

premalignant mammary tissues revealed that higher amounts of the NFκB components RelA and p50 in the nucleus, a higher level of phosphorylated IKK-β, and a lower level of IκBα in *Frs2β* ($^{+/+}$) tissues relative to *Frs-2β* ($^{-/-}$) tissues (Fig. 4 *D* and *E*). Moreover, immunohistochemistry revealed that RelA was localized to the nucleus in a much greater proportion of *Frs2β* ($^{+/+}$) than *Frs2β* ($^{-/-}$) premalignant luminal cells (Fig. 4 *G*, *Left* and *Middle* and *H*; compare values indicated by left bar versus those of middle bar). Treatment with DHMEQ in vivo dramatically decreased the number of *Frs2β* ($^{+/+}$) premalignant luminal cells harboring RelA in the nucleus (Fig. 4 *F*, *G*, *Right*, and *H*; compare *Frs2β* ($^{+/+}$) and DHMEQ − versus *Frs2β* ($^{+/+}$) and DHMEQ +) and inhibited expression of *Igf1* and *Cxcl12* transcripts in premalignant mammary tissues (Fig. 4*I*). These results suggest that NF-κB activation in luminal cells plays important roles in the expression of IGF1 and CXCL12 in premalignant mammary epithelial cells in vivo. It thus appears that FRS-2β triggers activation of NF-κB in the premalignant luminal cells, thereby inducing the production of cytokines including IGF1 and CXCL12 that in turn activate NF-κB in an autocrine and/or paracrine manner to spread the effects of NF-κB activation to the surrounding mammary epithelial cells.

**IGF1 and CXCL12 Expressed in the Premalignant Mammary Epithelial Cells Play Key Roles in Tumorigenesis.** To determine whether IGF1 and CXCL12 expressed in premalignant mammary epithelial cells contribute to tumorigenesis, we treated *Frs2β* ($^{+/+}$) xenograft mice with the IGF1-neutralizing antibody or a combination of CXCR4 and CXCR7 inhibitors, which block both the receptors for CXCL12 (hereinafter called "CXCL12 inhibitor"). Treatment with either the IGF1-neutralizing antibody or the CXC12 inhibitor significantly suppressed tumorigenesis and combined treatment with the IGF1-neutralizing antibody, and the CXC12 inhibitor yielded the strongest suppression of tumor volume and weight (Fig. 4 *I–L*). We used effective doses of the inhibitors that were well tolerated without toxic effects, as previously reported (31, 32). These results indicate that the production of IGF1 and CXCL12 in premalignant mammary tissues creates a microenvironment that is necessary for tumorigenesis.

**FRE-2β and NEMO Are Colocalized on Early Endosomes in MMTV-ErbB2 (+) Mammary Epithelial Cells.** We next examined how FRS2β induces activation of NF-κB. Immunofluorescence staining for FRS2β showed a punctate cytoplasmic distribution in higher-magnification (Fig. 1*D*) reminiscent of its localization on intracellular vesicles, as previously reported (20). Similarly, it was reported that ErbB2 is localized not only on the plasma membrane but also on intracellular vesicles (33). To examine whether FRS2β is localized on the early endosomes, we stained cultured mammary epithelial cells derived from MMTV-ErbB2 (+)/*Frs2β* ($^{+/+}$) mice or MMTV-ErbB2 (−)/*Frs2β* ($^{+/+}$) wild-type mice with antibodies against FRS2β and an early endosomal marker EEA1. These antibodies were validated in this study (Fig. 1*D* and *SI Appendix*, Figs. S1 *C*, *G*, *I* and S2*G*) and in previous studies (34). We examined colocalization of FRS2β and EEA1 in FRS2β–positive cells. Higher levels of colocalization of FRS2β and EEA1 were observed in cells derived from MMTV-ErbB2 (+)/*Frs2β* ($^{+/+}$) than MMTV-ErbB2 (−)/*Frs2β* ($^{+/+}$) wild-type mice (Fig. 5*A*), indicating that FRS2β is localized on the early endosomes more efficiently in ErbB2-overexpressing cells. These results suggest that ErbB2 transported from the plasma membrane recruits FRS2β on the early endosomes since FRS2β binds to ErbB2 (15). This finding led us to hypothesize that ErbB2–FRS2β triggers activation of NF-κB on the early endosomes.

We focused on NEMO, a scaffold subunit of the IKK complex (3). To demonstrate the specificity of the anti-NEMO antibodies, we compared the immunofluorescent staining of cells following RNA interference knockdown of *Nemo*. Immunofluorescence staining with anti-NEMO antibodies showed a punctate cytoplasmic distribution, which was abolished following *Nemo* knockdown (*SI Appendix*, Fig. S9 *A* and *B*). We thus confirmed the specificity of the anti-NEMO antibody. We next stained cells derived from MMTV-ErbB2 (+)/*Frs2β* ($^{+/+}$) mice with antibodies against NEMO and EEA1. Notably, higher levels of colocalization of NEMO and EEA1 were observed in FRS2β–positive cells than in FRS2β-negative cells (Fig. 5*B*). This suggests that NEMO is localized on early endosomes more efficiently in FRS2β-expressing cells. These cells were stained with antibodies against TAK1, an upstream activator of the IKK complex, or IKK-β and EEA1. Higher levels of colocalization of TAK1 or IKK-β and EEA1 were observed in FRS2β-positive cells than in FRS2β-negative cells (*SI Appendix*, Fig. S9 *C* and *D*). This suggests that TAK1 and IKK-β are also more efficiently localized on early endosomes in FRS2β-expressing cells. We further stained cells derived from MMTV-ErbB2 (+)/*Frs2β* ($^{+/+}$) or MMTV-ErbB2 (−)/*Frs2β* ($^{+/+}$) wild-type mice and examined the colocalization of NEMO and EEA1 in FRS2β–positive cells. We found a greater degree of colocalization between NEMO and EEA1 in ErbB2-overexpressing cells (Fig. 5*C*). Finally, elevated colocalization of FRS2β and NEMO on early endosomes was observed in cells derived from MMTV-ErbB2 (+)/*Frs2β* ($^{+/+}$) mice than MMTV-ErbB2 (−)/*Frsβ* ($^{+/+}$) wild-type mice (Fig. 5*D*). Collectively, it is likely that FRS2β facilitates recruitment of TAK1 and IKK complex that includes NEMO and IKK-β to the early endosomes, resulting in the activation of the IKK complex (Fig. 5*E* and *SI Appendix*, Fig. S9*E*).

**Breast Cancer Tissues that Express High Levels of FRS-2β Harbor More Stroma.** We next examined *Frs2β* ($^{+/+}$) and *Frs2β* ($^{-/-}$) mammary tumors during malignant progression (Fig. 1 *G–I*). Immunohistochemistry revealed that a few FRS2β-positive tumor cells were observed in *Frs2β* ($^{+/+}$) tumor tissues, while no FRS2β–positive cells were observed in *Frs2β* ($^{-/-}$) tumor tissues as expected (Fig. 6*A*). Since CSCs are thought to originate from luminal progenitor cells (24, 35), it is reasonable to assume that FRS2β is expressed in a part of CSCs and tumor cells. Expression levels of *Igf1* and *Cxcl12* transcripts were higher in *Frs2β* ($^{\pm}$) tumors than in *Frs2β* ($^{-/-}$) tumors (Fig. 6*B*). Immunohistochemistry confirmed that expression levels of IGF1 and CXCL12 were higher in *Frs2β* ($^{+/+}$) tumors than in *Frs2β* ($^{-/-}$) tumors (Fig. 6 *C* and *D*). The efficiency of tumor sphere formation was greater in *Frs2β* ($^{+/+}$) tumor cells than in *Frs2β* ($^{-/-}$) tumor cells (*SI Appendix*, Fig. S10 *A* and *B*). *Frs2β* ($^{+/+}$) tumor sphere formation was diminished by treatment with inhibitors for IGF1 receptor, a receptor for IGF1, linsitinib, or AEW541 (*SI Appendix*, Fig. S10 *C* and *D*). These findings suggest that IGF1 derived from tumors cells support CSC growth. We further examined whether IGF1 and CXCL12 contributed to CSC growth using knockdown of *Igf1* and *Cxcl12* by siRNAs in tumor cells. We found that the efficiency of tumor sphere formation was significantly diminished in cells after the knockdown (*SI Appendix*, Fig. S10 *E–H*). These results suggest that both IGF1 and CXCL12 in tumor cells contribute to the growth of CSCs and tumorigenesis. Collectively, FRS-2β expressed not only in premalignant epithelial cells but also in tumor cells may contribute to IGF1 and CXCL12 production, leading to CSC growth and establishment of the stroma-rich tumor microenvironment during malignant progression.

Finally, we examined the expression of FRS2β in human breast cancer tissues in tissue array by immunohistochemistry. There was a positive correlation between expression levels of FRS2β and the amount of stroma (Fig. 6 *E* and *F*). Furthermore, the analysis of published gene expression profiles (36) revealed

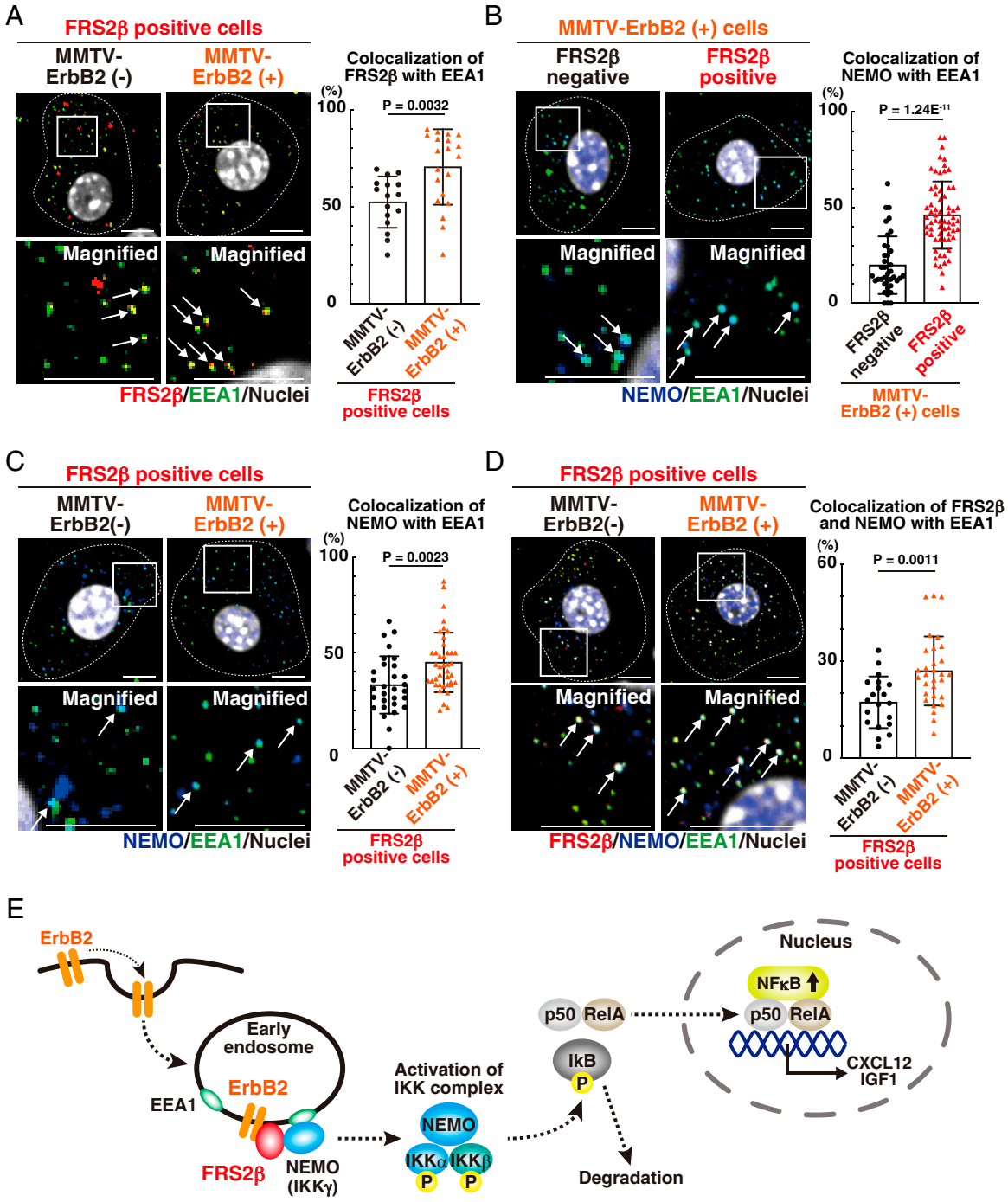


**Fig. 5.** FRS2β and NEMO are colocalized on the early endosomes in ErbB2-expressing mammary epithelial cells. (*A*, *Left*) Immunofluorescence staining for MMTV-ErbB2(−)/*Frs2β* ($^{+/+}$) wild-type cells and MMTV-ErbB2 (+)/*Frs2β* ($^{+/+}$) cells by anti–FRS2β (red) and anti-EEA1 (green) antibodies. Cells with >20 FRS2β puncta were defined as FRS2β–positive cells, while cells with <20 FRS2β puncta were defined as FRS2β–negative cells. Nuclei were stained by DAPI. The arrows indicate the puncta representing colocalization of FRS2β and EEA1. (*Right*) Quantification of the percentage of colocalized FRS2β and EEA1 puncta to total number of EEA1 puncta. $n = 16$ cells for MMTV-ErbB2 (−) and $n = 20$ cells for MMTV-ErbB2 (+) were counted. (*B*, *Left*) Immunofluorescence staining for FRS2β–positive and FRS2β–negative cells by anti-NEMO (blue) and anti-EEA1 (green) antibodies. The arrows indicate the puncta representing the colocalization of NEMO and EEA1. (*Right*) Quantification of the percentage of colocalized NEMO and EEA1 puncta to total number of EEA1 puncta. $n = 38$ FRS2β-negative cells and $n = 68$ FRS2β–positive cells were counted. (*C*, *Left*) Immunofluorescence staining for MMTV-ErbB2 (−)/*Frs2β* ($^{+/+}$) wild-type cells and MMTV-ErbB2 (+)/*Frs2β* ($^{+/+}$) cells by anti-NEMO (blue) and anti-EEA1 (green) antibodies. Nuclei were stained by DAPI. The arrows indicate the colocalized puncta. (*Right*) Quantification of the percentage of colocalized NEMO and EEA1 puncta to total number of EEA1 puncta. $n = 29$ cells for MMTV-ErbB2 (−) and $n = 44$ cells for MMTV-ErbB2 (+) were counted. (*D*, *Left*) Immunofluorescence staining for MMTV-ErbB2(−)/*Frs2β* ($^{+/+}$) wild-type cells and MMTV-ErbB2 (+)/*Frs2β* ($^{+/+}$) cells by anti–FRS2β (red), anti-NEMO (blue), and anti-EEA1 (green) antibodies. Nuclei were stained by DAPI. The arrows indicate the triple-positive puncta representing colocalization of FRS2β, NEMO, and EEA1. (*Right*) Quantification of the percentage of colocalized FRS2β, NEMO, and EEA1 puncta to total number of EEA1 puncta. $n = 23$ cells for MMTV-neu/ErbB2 (−) and $n = 30$ cells for MMTV-ErbB2 (+) were counted. (*E*) Schematic showing the interaction of ErbB2–FRS2β with NEMO on early endosomes, leading to activation of NF-κB. (*A–D*) Statistical significance was determined by unpaired, two-tailed Student's *t* test. Results are shown as means ± SD. (Scale bars, 5 μm.) All the immunofluorescence analyses in this figure are representative of at least three biologically independent experiments.

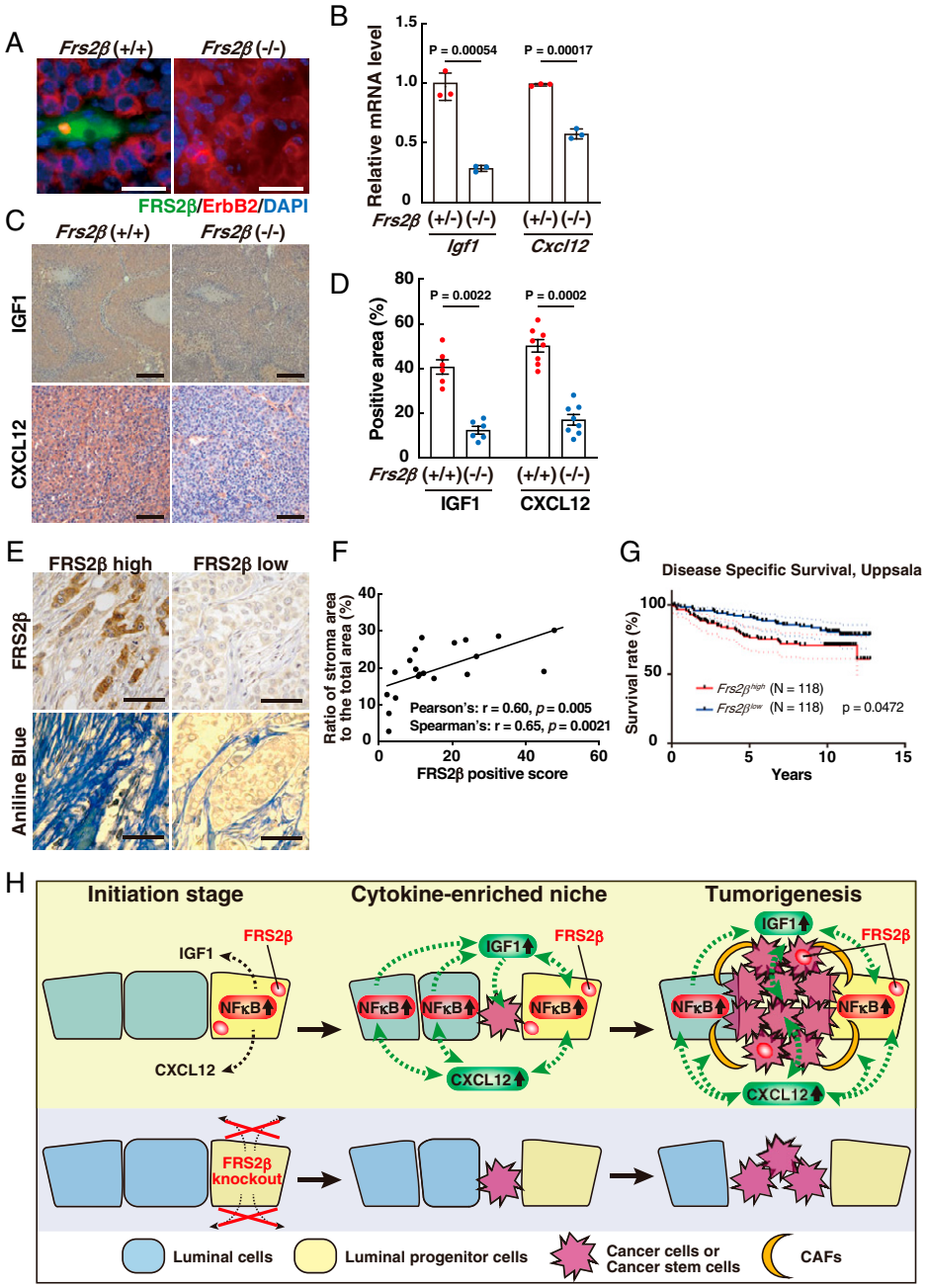


**Fig. 6.** Breast cancer tissues that express high levels of FRS2β harbor more stroma. (*A*) Representative images of immunofluorescence staining of MMTV-ErbB2 (+)/*Frs-2β* ($^{+/+}$) tumor tissues (*Right*) and MMTV-ErbB2 (+)/*Frs2β* ($^{-/-}$) tumor tissues using antibodies against FRS2β and ErbB2. Nuclei were stained by DAPI. (Scale bar, 25 μm.) (*B*) Expression levels of the indicated gene transcripts were compared between *Frs2β* ($^{\pm}$) and *Frs2β* ($^{-/-}$) tumor tissues using qPCR. Values were normalized to 18S rRNA, and fold changes were calculated relative to the values of *Frs-2β* ($^{\pm}$). Statistical significance was determined by unpaired, two-tailed Student's *t* test. Results are shown as means ± SD. $n = 3$ samples per genotype. (*C*) Representative images of immunohistochemical staining of *Frs2β* ($^{+/+}$) and *Frs2β* ($^{-/-}$) tumor tissues by using antibodies against IGF1 (*Top*) and CXCL12 (*Bottom*). (Scale bar, 100 μm [*Top*] and 50 μm [*Bottom*].) (*D*) Quantification of percentage of positive cells within *Frs2β* ($^{+/+}$) and *Frs2β* ($^{-/-}$) tumor tissues. $n = 6$ random fields for IGF1, and $n = 8$ random fields for CXC12 per genotype. $n = 3$ samples per genotype. Statistical significance was determined by two-tailed Mann–Whitney *U* test. Results are shown as means ± SEM. (*E*) Representative immunohistochemical staining for tissue array of human breast cancer using antibodies against FRS2β (*Top*) and aniline blue staining to detect collagen in stroma in the same tissues (*Bottom*). Breast cancer tissues with high levels (*Left*) or low levels (*Right*) of expression of FRS2β are shown. (Scale bar, 50 μm.) (*F*) Scatter plots showing the correlation between expression levels of FRS2β (FRS2β–positive score) in tumor cells and amount of stroma in tumor tissues. $n = 19$ tumor tissues. Pearson's or Spearman's correlation coefficient was calculated. (*G*) Kaplan–Meier survival curve, generated using the Uppsala cohort (GSE3494). Medians were used for cutoff value. *P* value was obtained by log-rank test. (*H*) Schematic showing FRS2β plays critical roles for creation of the cytokine-enriched niche that is required for mammary tumorigenesis with ample amount of stroma.

that patients with higher expression levels of *FRS2β* in breast cancer tissues had poorer prognosis (Fig. 6*G*). Since the dataset included information about immunohistochemical staining for estrogen and progesterone receptors in cancer tissues, we stratified the patients with or without these receptors in their cancer tissues. We found that higher-expression levels of *FRS2β* had a poorer prognosis among patients with estrogen or progesterone-positive breast cancer (*SI Appendix*, Fig. S11 *A–D*).

We analyzed expression levels of *FRS2β* in different subtypes of breast cancer tissues using a METABLIC dataset consisting of 2,000 primary breast cancers (37). Expression levels of *FRS2β* were significantly lower in the HER2-positive subtype than in other subtypes (*SI Appendix*, Fig. S11*E*). To further stratify the HER2 subtype, we used another method, expression-based classification (37). We found that expression levels of *FRS2β* were significantly lower in HER2-positive and hormone receptor–negative subtype than in other subtypes (*SI Appendix*, Fig. S11*F*). These findings raise the hypothesis that a lower amount of FRS2β might be sufficient for HER2-positive breast cancer tissues and that hormone receptor signaling might contribute to an increase in the expression levels of *FRS2β*.

## Discussion

In this study, we demonstrated that FRS2β is expressed in a small subset of luminal cells that include progenitor cells in the mammary tissues and is localized on the early endosomes together with the ErbB2 transported from the plasma membrane. FRS2β may interact with NEMO and trigger activation of IKK complex, leading to activation of NF-κB. As a result, various cytokines including CXCL12 and IGF1 are produced (Figs. 5*E* and 6 *H*, *Left*, "Initiation stage"). CXCL12 may stimulate surrounding cells through an autocrine and paracrine loop that amplifies intracellular NF-κB signaling. Concurrently, IGF1 would stimulate proliferation of stem/progenitor cells in an autocrine and paracrine manner. After a long latency in association with the chronic inflammatory changes, a cytokine-rich microenvironment is established that constitutes a preneoplastic state (Fig. 6 *H*, *Middle*, "Cytokine-enriched niche"). This would promote the growth of CSCs at their appearance to generate tumor cells with the help of CXCL12-mobilized stromal cells that would over time developed into CAFs (Fig. 6 *H*, *Right*, "Tumorigenesis"). In the absence of FRS2β, cytokines production is suppressed and a favorable premalignant microenvironment is prevented, which would restrict growth of CSCs and tumor cells. In addition, we elucidated that the combinatorial targeting of IGF1 and CXCL12 would effectively prevent tumorigenesis at an early stage.

Activated ErbB2s are transported into the early endosomes from the plasma membrane and undergo either recycling in the plasma membrane or degradation in the late endosomes and then lysosomes. It is thought that early endosomes serve as platforms for receptor signaling (14). We provide evidence that ErbB2–FRS2β recruits NEMO to the early endosomes, which leads to the activation of the IKK complex. In late endosomes or lysosomes, it is likely that the ErbB2–FRS2β binds to CIN85, which binds to the E3 ubiquitin ligase Cbl for degradation, as we reported previously (38). FRS2β also binds to phosphorylate ERK, sequestering ERK in the cytoplasm and preventing its translocation to the nucleus (15).

It is known that RANK, a member of the TNF receptor superfamily, plays important roles for pregnancy-induced proliferation of ductal cells and alveolar formation (39). RANK activates TNF receptor–associated factor (TRAF) 6, an E3 ubiquitin ligase, which generates Lys63-linked ubiquitin chains on IKK complex, leading to activation of NF-κB (40). Considering that expression of TRAF6 is increased in luminal epithelial cells during pregnancy, it is possible that TRAF6 is involved in FRS2β-mediated NF-κB activation. To elucidate the precise molecular mechanisms, further analysis will be required.

Based on the pathological analysis, human breast cancer begins with the hyperplasia of epithelial cells, then ductal carcinoma in situ (DCIS), and finally invasive carcinoma (6). It is reported that genes involved in inflammatory response are up-regulated in the invasive type of DCIS (41), consistent with our finding that chronic inflammation takes place before the onset of the disease.

Several studies have reported that FRS2β have functions acting as an adaptor protein to transmit signals emanating from FGF receptors and neurotrophin receptors, which are redundant functions already performed by the FRS2 family member FRS2α (42–45). Although the mutant mice in which the *Frs2α* gene is disrupted show embryonic lethality (46–48), in this study, we showed that the mutant mice in which *Frs2β* is disrupted show minimal phenotype in physiological conditions. This is probably due to the compensation by FRS2α for the loss of FRS2β (49).

FRS2β deficiency might cause a rapid reduction in mammary glands due to aging, since the growth ability of luminal progenitor cells is decreased. It is reasonable to speculate that FRS2β prevents the depletion of luminal progenitor cells by increasing the levels of cytokines, such as IGF1, which are required for their maintenance under normal physiological conditions.

In conclusion, this study presents an angle to develop preventive strategies for breast cancer by targeting the inflammatory premalignant microenvironment: the FRS2β–NF-κB pathway or its downstream cytokines, IGF1 and CXCL12.

## Materials and Methods

**Statistical Analyses.** All images and data shown are representative of several experiments performed on different days. Each experiment was repeated independently with similar results. Statistics were computed using GraphPad Prism (version 8). For normally distributed datasets, significance was calculated by unpaired, two-tailed Student's *t* test. Data are presented as means ± SEM or means ± SD. For nonparametric datasets, Mann–Whitney *U* tests were performed. Data are presented as means ± SEM or means ± SD. The tumor growth datasets were analyzed using the Bonferroni-corrected two-way ANOVA to compute statistical significance. Data are presented as means ± SEM. Tumor-initiating cell frequency was analyzed by Extreme Limiting Dilution Analysis software (bioinf.wehi.edu.au/software/elda/). The quantification of immunoblotting results was performed using ImageJ software. Kaplan–Meier survival curves were analyzed by log-rank test. Quantification of staining results of tissue array was performed using WinROOF software. Pearson's and Spearman's correlation (two sided) were performed to determine correlation between expression levels of FRS-2β in tumor cells and amount of stroma in tumor tissues.

**Study Approval.** Mice were handled according to the guidelines of the Institute of Medical Science at The University of Tokyo and Kanazawa University. The experiments were approved by the ethics committees for Animal Research at the Institute of Medical Science, The University of Tokyo, and Kanazawa University.

**Data Availability.** DNA microarray data have been deposited in Gene Expression Omnibus (GSE120034).

**ACKNOWLEDGMENTS.** We are grateful to M. Watanabe (Institute of Medical Science, The University of Tokyo) for technical support and to H. Nakauchi, Y. Ishii, and A. Fujita (Institute of Medical Science, The University of Tokyo) for their help with flow cytometry. We are thankful to ChemoCentryx, Inc. for kindly providing CCX771 and to K. Umezawa (Aichi Medical University) for kindly providing DHMEQ. This work was supported in part by an Extramural Collaborative Research Grant from the Cancer Research Institute at Kanazawa University, the Ministry of Education, Culture, Sports, Science, and Technology KAKENHI Grant Number. 22130009 and 20H05029; the Japan Soceity for Promotion of Science KAKENHI Grant Number. JP17K19587, JP18H02679, JP19K22557, and JP21H02761; and a research grant from AMED Project for Cancer Research and Therapeutic Evolution (Grant Number. 19193063 and 21446781) to N.G.

1. R. L. Siegel, K. D. Miller, A. Jemal, Cancer statistics, 2019. *CA Cancer J. Clin.* **69**, 7–34 (2019).
2. J. Cuzick, Preventive therapy for cancer. *Lancet Oncol.* **18**, e472–e482 (2017).
3. M. Karin, F. R. Greten, NF-kappaB: Linking inflammation and immunity to cancer development and progression. *Nat. Rev. Immunol.* **5**, 749–759 (2005).
4. H. Zahid, E. R. Simpson, K. A. Brown, Inflammation, dysregulated metabolism and aromatase in obesity and breast cancer. *Curr. Opin. Pharmacol.* **31**, 90–96 (2016).
5. J. E. Visvader, J. Stingl, Mammary stem cells and the differentiation hierarchy: Current status and perspectives. *Genes Dev.* **28**, 1143–1158 (2014).

6. C. J. Fabian, B. F. Kimler, Breast cancer chemoprevention: Current challenges and a look toward the future. *Clin. Breast Cancer* **3**, 113–124 (2002).
7. P. S. Bhathal, R. W. Brown, G. C. Lesueur, I. S. Russell, Frequency of benign and malignant breast lesions in 207 consecutive autopsies in Australian women. *Br. J. Cancer* **51**, 271–278 (1985).
8. K. Chin *et al.*, Genomic and transcriptional aberrations linked to breast cancer pathophysiologies. *Cancer Cell* **10**, 529–541 (2006).
9. Y. Yarden, M. X. Sliwkowski, Untangling the ErbB signalling network. *Nat. Rev. Mol. Cell Biol.* **2**, 127–137 (2001).
10. C. T. Guy *et al.*, Expression of the neu protooncogene in the mammary epithelium of transgenic mice induces metastatic disease. *Proc. Natl. Acad. Sci. U.S.A.* **89**, 10578–10582 (1992).
11. A. Cicalese *et al.*, The tumor suppressor p53 regulates polarity of self-renewing divisions in mammary stem cells. *Cell* **138**, 1083–1095 (2009).
12. P. Meijnen, J. L. Peterse, N. Antonini, E. J. Rutgers, M. J. van de Vijver, Immunohistochemical categorisation of ductal carcinoma in situ of the breast. *Br. J. Cancer* **98**, 137–142 (2008).
13. A. Sorkin, M. von Zastrow, Endocytosis and signalling: Intertwining molecular networks. *Nat. Rev. Mol. Cell Biol.* **10**, 609–622 (2009).
14. H. W. Platta, H. Stenmark, Endocytosis and signaling. *Curr. Opin. Cell Biol.* **23**, 393–403 (2011).
15. D. Iejima *et al.*, FRS2beta, a potential prognostic gene for non-small cell lung cancer, encodes a feedback inhibitor of EGF receptor family members by ERK binding. *Oncogene* **29**, 3087–3099 (2010).
16. N. Gotoh, S. Laks, M. Nakashima, I. Lax, J. Schlessinger, FRS2 family docking proteins with overlapping roles in activation of MAP kinase have distinct spatial-temporal patterns of expression of their transcripts. *FEBS Lett.* **564**, 14–18 (2004).
17. K. McDougall, C. Kubu, J. M. Verdi, S. O. Meakin, Developmental expression patterns of the signaling adapters FRS-2 and FRS-3 during early embryogenesis. *Mech. Dev.* **103**, 145–148 (2001).
18. K. Hinohara *et al.*, ErbB receptor tyrosine kinase/NF-κB signaling controls mammosphere formation in human breast cancer. *Proc. Natl. Acad. Sci. U.S.A.* **109**, 6584–6589 (2012).
19. E. Sahai *et al.*, A framework for advancing our understanding of cancer-associated fibroblasts. *Nat. Rev. Cancer* **20**, 174–186 (2020).
20. Y. Minegishi *et al.*, Prominent expression of FRS2beta protein in neural cells and its association with intracellular vesicles. *FEBS Lett.* **583**, 807–814 (2009).
21. A. Van Keymeulen *et al.*, Distinct stem cells contribute to mammary gland development and maintenance. *Nature* **479**, 189–193 (2011).
22. Y. Inoue *et al.*, Imaging living mice using a 1-T compact MRI system. *J. Magn. Reson. Imaging* **24**, 901–907 (2006).
23. D. J. Dabbs, *Breast Pathology* (Elsevier, ed. 2, 2016).
24. J. C. Liu, T. Deng, R. S. Lehal, J. Kim, E. Zacksenhaus, Identification of tumorsphere- and tumor-initiating cells in HER2/Neu-induced mammary tumors. *Cancer Res.* **67**, 8671–8681 (2007).
25. C. Saygin, D. Matei, R. Majeti, O. Reizes, J. D. Lathia, Targeting cancer stemness in the clinic: From hype to hope. *Cell Stem Cell* **24**, 25–40 (2019).
26. J. Stingl *et al.*, Purification and unique properties of mammary epithelial stem cells. *Nature* **439**, 993–997 (2006).
27. F. Vaillant *et al.*, The mammary progenitor marker CD61/beta3 integrin identifies cancer stem cells in mouse models of mammary tumorigenesis. *Cancer Res.* **68**, 7711–7717 (2008).
28. G. Dontu *et al.*, In vitro propagation and transcriptional profiling of human mammary stem/progenitor cells. *Genes Dev.* **17**, 1253–1270 (2003).
29. F. Calvo *et al.*, Mechanotransduction and YAP-dependent matrix remodelling is required for the generation and maintenance of cancer-associated fibroblasts. *Nat. Cell Biol.* **15**, 637–646 (2013).
30. D. G. Duda *et al.*, CXCL12 (SDF1alpha)-CXCR4/CXCR7 pathway inhibition: An emerging sensitizer for anticancer therapies? *Clin. Cancer Res.* **17**, 2074–2080 (2011).
31. R. Matsusue *et al.*, Hepatic stellate cells promote liver metastasis of colon cancer cells by the action of SDF-1/CXCR4 axis. *Ann. Surg. Oncol.* **16**, 2645–2653 (2009).
32. K. Yamada *et al.*, CXCL12-CXCR7 axis is important for tumor endothelial cell angiogenic property. *Int. J. Cancer* **137**, 2825–2836 (2015).
33. R. Worthylake, L. K. Opresko, H. S. Wiley, ErbB-2 amplification inhibits down-regulation and induces constitutive activation of both ErbB-2 and epidermal growth factor receptors. *J. Biol. Chem.* **274**, 8865–8874 (1999).
34. H. Maib, F. Ferreira, S. Vassilopoulos, E. Smythe, Cargo regulates clathrin-coated pit invagination via clathrin light chain phosphorylation. *J. Cell Biol.* **217**, 4253–4266 (2018).
35. E. Lim *et al.*; kConFab, Aberrant luminal progenitors as the candidate target population for basal tumor development in BRCA1 mutation carriers. *Nat. Med.* **15**, 907–913 (2009).
36. C. Desmedt *et al.*; TRANSBIG Consortium, Strong time dependence of the 76-gene prognostic signature for node-negative breast cancer patients in the TRANSBIG multicenter independent validation series. *Clin. Cancer Res.* **13**, 3207–3214 (2007).
37. C. Curtis *et al.*; METABRIC Group, The genomic and transcriptomic architecture of 2,000 breast tumours reveals novel subgroups. *Nature* **486**, 346–352 (2012).
38. Y. Minegishi *et al.*, Adaptor protein complex of FRS2β and CIN85/CD2AP provides a novel mechanism for ErbB2/HER2 protein downregulation. *Cancer Sci.* **104**, 345–352 (2013).
39. J. E. Fata *et al.*, The osteoclast differentiation factor osteoprotegerin-ligand is essential for mammary gland development. *Cell* **103**, 41–50 (2000).
40. M. Yamamoto *et al.*, TRAF6 maintains mammary stem cells and promotes pregnancy-induced mammary epithelial cell expansion. *Commun. Biol.* **2**, 292 (2019).
41. R. Lesurf *et al.*; Oslo Breast Cancer Research Consortium (OSBREAC), Molecular features of subtype-specific progression from ductal carcinoma in situ to invasive breast cancer. *Cell Rep.* **16**, 1166–1179 (2016).
42. N. Gotoh, Regulation of growth factor signaling by FRS2 family docking/scaffold adaptor proteins. *Cancer Sci.* **99**, 1319–1325 (2008).
43. S. Nandi, K. Alviña, P. J. Lituma, P. E. Castillo, J. M. Hébert, Neurotrophin and FGF signaling adapter proteins, FRS2 and FRS3, regulate dentate ranule cell maturation and excitatory synaptogenesis. *Neuroscience* **369**, 192–201 (2018).
44. S. Wu *et al.*, Whole-genome sequencing identifies ADGRG6 enhancer mutations and FRS2 duplications as angiogenesis-related drivers in bladder cancer. *Nat. Commun.* **10**, 720 (2019).
45. E. Manchado *et al.*, A combinatorial strategy for treating KRAS-mutant lung cancer. *Nature* **534**, 647–651 (2016).
46. N. Gotoh *et al.*, The docking protein FRS2alpha is an essential component of multiple fibroblast growth factor responses during early mouse development. *Mol. Cell. Biol.* **25**, 4105–4116 (2005).
47. N. Gotoh *et al.*, Tyrosine phosphorylation sites on FRS2alpha responsible for Shp2 recruitment are critical for induction of lens and retina. *Proc. Natl. Acad. Sci. U.S.A.* **101**, 17144–17149 (2004).
48. S. Yamamoto *et al.*, Essential role of Shp2-binding sites on FRS2alpha for corticogenesis and for FGF2-dependent proliferation of neural progenitor cells. *Proc. Natl. Acad. Sci. U.S.A.* **102**, 15983–15988 (2005).
49. S. Nandi *et al.*, FGF-dependent, context-driven role for FRS adapters in the early telencephalon. *J. Neurosci.* **37**, 5690–5698 (2017).